Am J Cancer Res 2026;16(6):2278-2296
www.ajcr.us /ISSN:2156-6976/ajcr0173727

Original Article

RPS2 and EEF1B2 are associated with glycolysis-related malignant phenotypes in COAD

Jianbin Hou, Yangyang Dong, Huiyang Qian

Quanzhou First Hospital Affiliated to Fujian Medical University, Quanzhou 362000, Fujian, China

Received April 30, 2026; Accepted June 4, 2026; Epub June 15, 2026; Published June 30, 2026

Abstract: Lactate metabolism-related reprogramming is closely associated with colon adenocarcinoma (COAD) progression, but related key molecules remain unclear. This study integrated the colorectal cancer single-cell RNA sequencing dataset GSE231559, which served as a single-cell reference and integrated it with bulk RNA-seq data from TCGA-COAD to screen lactate metabolism-related candidate genes. Epithelial cells showed higher lactate metabolism-related transcriptional scores. An overlap-based screening strategy was applied, encompassing three gene sets: epithelial markers associated with lactate metabolism, dysregulated transcripts in the TCGA colon adenocarcinoma cohort, and genes within the co-expression module correlated with the lactate score. This analysis prioritized 14 genes for subsequent investigation. RPS2 and EEF1B2 were selected for further validation. Public database analysis and immunohistochemistry of paired tissues from 50 patients with COAD showed that RPS2 and EEF1B2 were highly expressed in tumor tissues. In HT-29 cells, siRNA-mediated knockdown of RPS2 or EEF1B2 reduced proliferation and migration, increased apoptosis, and decreased HK2, PFK1, PKM2, and LDHA expression, with stronger changes after double knockdown. RPS2 knockdown also increased residual glucose levels and reduced lactate release. Co-immunoprecipitation showed that RPS2 and EEF1B2 were detected in the same protein complex, and EEF1B2 overexpression partially rescued the effects of RPS2 knockdown. These findings suggest that RPS2 and EEF1B2 are associated with glycolysis-related malignant phenotypes in HT-29 cells.

Keywords: Colon adenocarcinoma, lactate metabolism, glycolysis, RPS2, EEF1B2, single-cell RNA sequencing

Introduction

According to the 2022 global cancer burden data reported by the International Agency for Research on Cancer, colorectal cancer is the third most commonly diagnosed malignancy worldwide and remains the second leading contributor to cancer-related mortality [1]. In recent years, improvements in surgery, chemotherapy, targeted therapy, and immunotherapy have enhanced outcomes for some patients. However, many patients with advanced CRC still experience recurrence, metastasis, and treatment resistance, leading to a poor prognosis. CRC primarily includes colon cancer and rectal cancer. Colon adenocarcinoma is the most common histological subtype, accounting for the largest proportion of CRC cases [2]. The development of COAD is influenced by many genes, signaling pathways, and the tumor microenvironment. Therefore, clarifying the molecular mechanisms of metastasis and identifying new biomarkers and therapeutic targets are crucial for improving patient prognosis.

Metabolic remodeling is an important feature of cancer. Aerobic glycolysis, commonly known as the Warburg effect, is a common metabolic change frequently observed during COAD progression. This effect has recently been recognized as an important therapeutic vulnerability in CRC [3, 4]. The Warburg effect describes a metabolic state in which cancer cells primarily rely on increased glucose intake and elevated glycolytic activity to support energy production and biosynthetic demands, even under oxygen-rich conditions. This heightened glycolysis leads to increased lactate release and export. As a result, lactate release-related molecules such as LDHA are often abnormally expressed during COAD progression [5], and these abnormal changes may also be associated with unfavorable biological behavior and altered treatment sensitivity in colon adenocarcinoma [6,

https://doi.org/10.62347/SWNV5972

7]. At the same time, enhanced glycolysis and lactate accumulation may promote each other, further reshape the tumor microenvironment, and participate in angiogenesis, immune suppression, invasion, metastasis, and treatment tolerance [4, 8-11]. Therefore, screening candidate molecules based on transcriptional features related to glycolysis and lactate metabolism may help clarify the molecular basis of metabolic abnormalities in COAD.

Based on this background, the present study used a colorectal cancer single-cell transcriptomic dataset as a reference to characterize lactate metabolism-related transcriptional features in tumor epithelial cells and integrated these findings with bulk RNA-seq data from the TCGA-COAD cohort. Using differential expression analysis together with weighted gene co-expression network analysis, we screened RPS2 and EEF1B2 as possible candidate molecules linked to lactate metabolism-related characteristics. We then performed public database validation, immunohistochemical analysis of clinical COAD tissues, in vitro functional experiments, and protein interaction assays to further assess the expression profiles and possible functional roles of RPS2 and EEF1B2 in COAD, as well as their association with glycolysis-related changes. This study aimed to provide clues for understanding the molecular basis of metabolic abnormalities in COAD.

Materials and methods

Public databases and bioinformatics analysis

Data acquisition and lactate metabolism-related gene set: The single-cell RNA sequencing dataset GSE231559 for CRC was retrieved from the Gene Expression Omnibus (GEO) database, including three primary colorectal cancer tissues and three matched normal colorectal tissues. Bulk transcriptome profiles and related clinical data for the TCGA-COAD cohort were collected from The Cancer Genome Atlas (TCGA). In this cohort, 286 tumor tissues and 43 normal tissues were used for differential expression analysis. Genes associated with lactate metabolism were extracted from the MSigDB database.

Single-cell RNA-seq processing and cell annotation: The GSE231559 scRNA-seq expression matrix was processed using the Seurat R package. Quality control was performed before downstream analysis. Genes expressed in fewer than three cells were excluded. Cells were then filtered using preset quality control criteria. Cells were retained only when they had 100-7,500 detected genes, more than 1,000 UMIs, and less than 10% mitochondrial gene content. After quality control, 28,617 cells remained for further analysis. Data were processed using the standard Seurat workflow. The Harmony R package was used to reduce batch effects among samples. Next, the 2,000 most variable genes were selected. These genes were used for principal component analysis. Cell clustering was performed using the first 40 principal components. The cell distribution was visualized by UMAP. Cluster marker genes were identified with the Seurat FindAllMarkers function. Cell types were annotated using these markers and known canonical markers. The identified cell types included T/NK cells, epithelial cells, monocytes/macrophages, B cells, fibroblasts, plasma cells, endothelial cells, and mast cells.

Lactate metabolism scoring and epithelial cell-based differential analysis: Single-sample gene set enrichment analysis (ssGSEA) was used to calculate the lactate metabolism score, referred to as the Lac score, for each single cell based on the lactate metabolism-related gene set. The Lac score served as a surrogate indicator of lactate metabolism-related transcriptional activity, rather than a direct measure of lactate production or metabolic flux. After comparing the Lac scores among major cell types, epithelial cells showed relatively higher lactate metabolism-related transcriptional scores and were therefore selected for further analysis. Epithelial cells were divided into high-Lac and low-Lac groups according to the median Lac score. Differential expression analysis between the high-Lac and low-Lac epithelial cell groups was performed using the FindMarkers function in Seurat. Genes differentially expressed between these two groups were considered epithelial cell-derived lactate metabolism-related marker genes and were used for subsequent integrative analysis.

Bulk RNA-seq analysis, differential expression analysis, and WGCNA: For the bulk RNA-seq analysis, the TCGA-COAD expression dataset was normalized before downstream analysis. Using the same lactate metabolism-related

gene set, we calculated a lactate metabolism score, defined as the Lac score, for each TCGA-COAD sample by single-sample gene set enrichment analysis. Weighted gene co-expression network analysis was then performed to screen gene modules associated with the Lac score. Before constructing the co-expression network, sample clustering was used to detect possible outliers, and no obvious outlier samples were removed. A soft-thresholding power of 16 was selected to approximate a scale-free network structure. After module construction, the relationship between each module and the Lac score was examined by module-trait correlation analysis. Ten co-expression modules were identified. Among them, the pink module contained 64 genes and showed the strongest positive correlation with the Lac score. Therefore, genes in this module were retained for subsequent candidate gene screening. In addition, differential expression analysis between TCGA-COAD tumor and normal tissues was conducted using the limma R package. Differentially expressed genes were defined using the criteria of false discovery rate < 0.05 and absolute log2 fold change ≥ 2. Under these thresholds, 2,315 differentially expressed genes were obtained.

Candidate gene screening: Candidate lactate metabolism-related genes were identified by intersecting three gene sets: epithelial cell-derived lactate metabolism-related marker genes from the single-cell analysis, differentially expressed genes between TCGA-COAD tumor and normal tissues, and genes from the Lac score-related WGCNA pink module. The intersection analysis identified 14 lactate metabolism-related candidate genes. Among these candidate genes, RPS2 and EEF1B2 were selected for further validation based on their expression patterns in COAD tissues, their association with lactate metabolism-related transcriptional features, their biological relevance to protein translation and tumor progression, and the predicted protein-level association suggested by STRING analysis.

Public expression validation and protein interaction prediction: For public expression validation, RPS2 and EEF1B2 expression levels were analyzed using a TCGA- and GTEx-based public expression platform. The comparison included 275 COAD tumor samples and 349 normal samples, and expression values were presented as log2(TPM + 1). After normalization, gene expression levels were compared between tumor and normal tissue samples. These analyses were used to provide transcriptomic-level evidence for the expression patterns of RPS2 and EEF1B2 before clinical tissue validation. The possible protein-level relationship between RPS2 and EEF1B2 was explored using the STRING database. The analysis was limited to Homo sapiens, and interactions were screened under a medium-confidence score threshold. STRING analysis was used only as a prediction of potential protein association. Co-immunoprecipitation experiments were then performed to examine whether RPS2 and EEF1B2 could be detected in the same protein complex in HT-29 cells.

Clinical samples and immunohistochemical analysis

Sample collection: Tumor tissues and matched adjacent non-tumor tissues were collected from 50 patients who underwent surgical resection for COAD. Eligible patients had a pathological diagnosis of colon adenocarcinoma and had not received preoperative radiotherapy, chemotherapy, targeted therapy, or immunotherapy. Patients with a previous history of other malignancies or incomplete tissue information were excluded. The collection and application of human tissue specimens were reviewed and approved by the Ethics Committee of Quanzhou First Hospital (Approval No. Quanyi Ethics [2025] K147; April 14, 2025). Written informed consent was obtained from all enrolled participants.

Immunohistochemical analysis: Paraffin tissue blocks were cut into 4 μm sections. The slides were dewaxed and hydrated. Antigen retrieval was performed in Tris-EDTA buffer at pH 9.0 by microwave heating for 15 min. Endogenous peroxidase was blocked with 3% H_2O_2. Nonspecific binding was blocked with 5% BSA. The sections were incubated overnight at 4°C with anti-RPS2 antibody (Abcam, Cambridge, UK; Cat. No. ab155961; 1:200) or anti-EEF1B2 antibody (Proteintech, Wuhan, China; Cat. No. 10095-2-AP; 1:200). The sections were then incubated with an HRP-conjugated goat anti-rabbit IgG secondary antibody (Proteintech, Wuhan, China; Cat. No. RGAR001; 1:10000) at

Table 1. Sequences of siRNAs

Target Name	Type	Sequence (5'-3')
si-RPS2-1	Sense	5'-GCAUCUACAUCUUCUCCAUTT-3'
	Antisense	5'-AUGGAGAAGAUGUAGAUGCTT-3'
si-RPS2-2	Sense	5'-CCAGUAUGCCACUAAGAUATT-3'
	Antisense	5'-UAUCUUAGUGGCAUACUGGTT-3'
si-EEF1B2-1	Sense	5'-GAGCUUCAUCAAGAAUAUATT-3'
	Antisense	5'-UAUAUUCUUGAUGAAGCUCTT-3'
si-EEF1B2-2	Sense	5'-GCAGCUGUGAUGAGUAUAATT-3'
	Antisense	5'-UUAUACUCAUCACAGCUGCTT-3'
si-NC	Sense	5'-UUCUCCGAACGUGUCACGUTT-3'
	Antisense	5'-ACGUGACACGUUCGGAGAATT-3'

37°C for 30 min. DAB was used for color development, and hematoxylin was used to stain nuclei. The slides were dehydrated, cleared, mounted, and observed under a light microscope. For quantification, five random fields were selected from each section at ×200 magnification. ImageJ was used to measure the positive staining area and the total tissue area. The positive area ratio was calculated. The mean value was used as the expression level of each sample.

Cell culture and transfection

HT-29 human COAD cells were purchased from Wuhan Procell Life Science & Technology Co., Ltd. (Wuhan, China; Cat. No. CL-0118). Cells were cultured in McCoy's 5A medium supplemented with 10% fetal bovine serum (Gibco, Grand Island, NY, USA; Cat. No. 10099-141) and 1% penicillin-streptomycin (Solarbio, Beijing, China; Cat. No. P1400) at 37°C with 5% CO_2 in a CO_2 incubator (Thermo Fisher Scientific, Waltham, MA, USA; Model 3111). For routine washing and digestion, 1×PBS (Servicebio, Wuhan, China; Cat. No. G4202-500ML) and trypsin-EDTA solution (Solarbio, Beijing, China; Cat. No. T1300) were used. For knockdown assays, cells were seeded and transfected at 60%-70% confluence. Four groups were included: si-NC, si-RPS2, si-EEF1B2, and combined si-RPS2/si-EEF1B2. In the co-silencing group, siRNAs against both genes were added simultaneously. Transfection was performed using Lipofectamine 6000 Transfection Reagent (Beyotime, Shanghai, China; Cat. No. C0526) in Opti-MEM medium (Servicebio, Wuhan, China; Cat. No. G4568-500ML) according to the manufacturer's protocol. Two siRNAs were screened for each gene, and the more efficient sequence was selected for subsequent experiments. After 48 h, cells were collected for qPCR, Western blotting, proliferation, apoptosis, migration, and glycolysis-related analyses.

To further examine the association between RPS2 and EEF1B2, HT-29 cells were divided into si-NC and si-RPS2 groups. Cells were collected 48 h after transfection to determine EEF1B2 expression, glycolysis-related metabolic alterations, and the possible protein interaction using co-immunoprecipitation.

For rescue assays, HT-29 cells were divided into four groups: si-NC + Vector, si-RPS2 + Vector, si-RPS2 + oe-EEF1B2, and oe-EEF1B2 alone. The EEF1B2 overexpression plasmid or empty vector was introduced into cells using Lipofectamine 6000 Transfection Reagent. In the si-RPS2 + oe-EEF1B2 group, cells were first treated with si-RPS2 and then transfected with the EEF1B2 overexpression plasmid. Cells were collected 48 h after plasmid transfection to verify rescue efficiency and to perform subsequent functional and metabolic analyses. The siRNA sequences used in this study are provided in **Table 1**.

qPCR and Western blot

Total RNA was extracted from treated cells using TRIzon Reagent (CWBIO, Beijing, China; Cat. No. 04106/32024) according to the manufacturer's instructions. Briefly, cells were lysed with TRIzon reagent, and chloroform was added at 0.2 mL per 1 mL TRIzon. After vigorous shaking and incubation at room temperature for 2-3 min, the samples were centrifuged at 12,000 rpm for 15 min at 4°C. The aqueous phase was transferred to a new RNase-free tube, mixed with an equal volume of isopropanol, and incubated at room temperature for 10 min. After centrifugation at 12,000 rpm for 10 min at 4°C, the RNA pellet was washed with 75% ethanol, air-dried, and dissolved in RNase-free water. RNA concentration and purity were measured using an ultramicro nucleic acid analyzer (Allsheng, Hangzhou, China; Model Nano-400).

For reverse transcription, cDNA was synthesized using NovoScript® Plus All-in-one 1st Strand cDNA Synthesis SuperMix (gDNA Purge)

Table 2. Primer sequences used for qPCR

Gene	Forward primer (5'-3')	Reverse primer (5'-3')
GAPDH	CATCACTGCCACCCAGAAGACTG	ATGCCAGTGAGCTTCCCGTTCAG
RPS2	CACTGGCATTGTCTCTGCTCCT	TGGAGATGGCATCAAAGGTGGC
EEF1B2	GTAGAAGACACCACAGGAAGTGG	ACTGTGCAAGGCGTTCTTCTCG
HK2	CCCTGTGAAGATGTTGCCCACT	CCTTCGCTTGCCATTACGCACG
PFK1	CTGTTCGCTCTACCGTGAGGAT	TTGGAACCACCTTGACCAGTCC
PKM2	CAGAGAAGGTCTTCCTGGCTCA	GCCACATCACTGCCTTCAGCAC
LDHA	ACGCAGACAAGGAGCAGTGGAA	ATGCTCTCAGCCAAGTCTGCCA

(Novoprotein, Suzhou, China; Cat. No. E047-01B). The reverse transcription reaction was performed in a 20 μL system containing total RNA (1 pg-1 μg), 1 μL gDNA Purge, 10 μL 2× NovoScript® Plus 1st Strand cDNA Synthesis SuperMix, and RNase-free ddH_2O to 20 μL. The reverse transcription program was 50°C for 15 min and 85°C for 5 s. The synthesized cDNA was used immediately for qPCR or stored at -20°C.

qRT-PCR was performed using NovoStart® Universal Fast SYBR qPCR SuperMix (Novoprotein, Suzhou, China; Cat. No. E401-01B) on a fluorescence quantitative PCR system (Bioer Technology, Hangzhou, China; Model FQD-96A). The qPCR reaction was performed in a 20 μL system containing 10 μL 2× NovoStart® Universal Fast SYBR qPCR SuperMix, 1 μL cDNA, 0.4 μL forward primer, 0.4 μL reverse primer, and 8.2 μL RNase-free ddH_2O. The three-step amplification program was as follows: initial denaturation at 95°C for 10 min; 40 cycles of denaturation at 95°C for 10 s, annealing at 60°C for 30 s, and extension at 72°C for 30 s. The detected genes included RPS2, EEF1B2, HK2, PFK1, PKM2, and LDHA. GAPDH was used as the internal control. Relative gene expression was calculated using the 2-ΔΔCt method. Primers were synthesized by Sangon Biotech Co., Ltd. (Shanghai, China), and the primer sequences are shown in **Table 2**.

For Western blotting, total cellular proteins were extracted using RIPA lysis buffer (Servicebio, Wuhan, China; Cat. No. G2002-30ML) supplemented with 1% protease inhibitor cocktail. After lysis, the samples were incubated on a shaker at 4°C for approximately 15 min and centrifuged at 12,000×g for 15 min at 4°C. The supernatants were collected as total cellular protein extracts and stored at -80°C until use. Protein concentration was determined using a BCA protein assay kit (Solarbio, Beijing, China; Cat. No. PC0020). Absorbance was measured at 562 nm using an automatic microplate reader (Biobase, Shandong, China; Model BK-EL10A). Equal amounts of protein were separated by 10%-12% SDS-PAGE. SDS-PAGE gels were prepared using Omni-Easy™ One-step PAGE Gel Fast Preparation Kit (Epizyme, Shanghai, China; Cat. No. PG222). A protein marker (Uelandy, Suzhou, China; Cat. No. P622M) was used to estimate molecular weight. Electrophoresis was performed using a vertical electrophoresis apparatus (Beijing Oriental Rayleigh Analytical Instrument Co., Ltd., Beijing, China; Model DYY-300D). Proteins were transferred onto PVDF membranes (Servicebio, Wuhan, China; Cat. No. G6050-0.45) using fast transfer buffer (Servicebio, Wuhan, China; Cat. No. G2028-1L) at a constant current of 300 mA.

After transfer, the membranes were blocked with protein-free rapid blocking buffer (Meilunbio, Dalian, China; Cat. No. MA0406) for 15 min. The membranes were then incubated overnight at 4°C with the following primary antibodies: anti-RPS2 antibody (Proteintech, Wuhan, China; Cat. No. 15562-1; 1:1000), anti-EEF1B2 antibody (Proteintech, Wuhan, China; Cat. No. 10483-1; 1:1000), anti-cleaved caspase-3 antibody (Proteintech, Wuhan, China; Cat. No. 20538-1; 1:1000), anti-Bax antibody (Proteintech, Wuhan, China; Cat. No. 50599-1; 1:60000), anti-Bcl-2 antibody (Proteintech, Wuhan, China; Cat. No. 80313; 1:20000), anti-HK2 antibody (Proteintech, Wuhan, China; Cat. No. 22029-1; 1:10000), anti-PFK1 antibody (Proteintech, Wuhan, China; Cat. No. 55028-1; 1:8000), anti-PKM2 antibody (Proteintech, Wuhan, China; Cat. No. 10078; 1:2000), anti-LDHA antibody (Proteintech, Wuhan, China; Cat. No. 21799; 1:10000), and anti-β-actin antibody (Proteintech, Wuhan, China; Cat. No. 66009-1-Ig; 1:50000). After washing with TBST, the membranes were incubated with HRP-conjugated goat anti-rabbit IgG (Proteintech, Wuhan, China; Cat. No. RGAR001; 1:10000) or HRP-conjugated goat anti-mouse IgG (Proteintech, Wuhan, China; Cat. No. RGAM001; 1:10000) for 1 h at room tempera-

ture. TBS powder (Servicebio, Wuhan, China; Cat. No. G0001-2L) and Tween-20 (Meilunbio, Dalian, China; Cat. No. MB2483-1) were used to prepare TBST. Protein bands were detected using Meilunbio® fg super sensitive ECL luminescence reagent (Meilunbio, Dalian, China; Cat. No. MA0186) and imaged with an automatic chemiluminescence image analysis system (Servicebio, Wuhan, China; Model SCG-W2000). Band gray values were analyzed using ImageJ software.

Cell functional assays

CCK-8 proliferation assay: Cell viability was measured using a CCK-8 assay kit (GLPBIO, Montclair, CA, USA; Cat. No. GK10001). Cells were seeded in 96-well plates. Each well contained 2,000 cells. Cell viability was measured at 0, 24, 48, and 72 h. At each time point, 10 μL CCK-8 solution was added to each well. Cells were incubated at 37°C for 2 h, and absorbance was measured at 450 nm using an automatic microplate reader (Beijing Liuyi Biotechnology Co., Ltd., Beijing, China; Model WD-2102B).

Flow cytometric apoptosis assay: Cell apoptosis was measured using an Annexin V-FITC/PI Apoptosis Kit (Beyotime, Shanghai, China; Cat. No. C1062L). Cells from each group were collected and stained according to the manufacturer's protocol. Briefly, cells were centrifuged at 300×g for 5 min, washed once with PBS, and resuspended in 100 μL 1× Annexin V binding buffer. Then, 2.5 μL Annexin V-FITC reagent and 2.5 μL PI reagent were added. The samples were incubated in the dark for 15-20 min at room temperature. After adding 400 μL 1× Annexin V binding buffer, the samples were analyzed using a flow cytometer (RaiseCare, China; Model RaiseCyte 2L6C). Early apoptotic cells and late apoptotic cells were counted, and their sum was used as the total apoptosis rate.

Transwell migration assay: Cell migration was assessed using 24-well Transwell chambers (BKMANLAB, China; Cat. No. 110304027). After treatment, 2×10^4 cells were suspended in serum-free medium and added to the upper chamber. Complete medium containing 10% FBS was added to the lower chamber. After 24 h, cells on the upper surface of the membrane were removed. Migrated cells on the lower surface were fixed with 4% paraformaldehyde (Servicebio, Wuhan, China; Cat. No. G1101-500ML) at room temperature for 15 min and stained with crystal violet staining solution (Servicebio, Wuhan, China; Cat. No. G1014-50ML). The migrated cells were observed and photographed using an inverted fluorescence microscope (Leica, Wetzlar, Germany; Model DMI4000B). Five random fields were counted for each insert, and the mean number of migrated cells was used for analysis.

Measurement of residual glucose level and lactate release: After treatment, cells were cultured in fresh complete medium for 24 h. The conditioned medium was then collected and centrifuged to remove cell debris. Glucose and lactate levels in the supernatant were measured using commercial kits. The glucose kit was from Aidisheng. The catalog number was ADS-W-TDX002. The lactate kit was also from Aidisheng. The catalog number was ADS-W-T009-96. All values were normalized to total cellular protein. This step was used to reduce the effect of differences in cell number.

Co-immunoprecipitation (Co-IP) assay

Co-immunoprecipitation was performed using a Pierce co-immunoprecipitation kit (Thermo Fisher Scientific, Waltham, MA, USA; Cat. No. 88805) according to the manufacturer's protocol. Briefly, 25 μL Protein A/G magnetic beads were incubated with 5 μg anti-RPS2 antibody (Invitrogen/Thermo Fisher Scientific; Cat. No. PA5-75565), anti-EEF1B2 antibody (Proteintech, Wuhan, China; Cat. No. 10483-1-AP), or anti-rabbit IgG control (Cat. No. 7074) for antibody coupling. HT-29 cells were lysed with immunoprecipitation lysis/wash buffer containing protease and phosphatase inhibitors. The lysates were centrifuged at approximately 13,000×g for 10 min, and equal amounts of protein lysate were incubated with antibody-coupled magnetic beads overnight at 4°C. After washing, bound proteins were eluted, denatured with loading buffer and DTT at 95-100°C for approximately 5 min, and analyzed by Western blotting. PVDF membranes (Millipore, Burlington, MA, USA; Cat. No. IPVH00010) were used for protein transfer. HRP-conjugated goat anti-rabbit IgG (ZSGB-BIO, Beijing, China; Cat. No. ZB-2301; 1:2000), HRP-conjugated goat anti-mouse IgG (ZSGB-BIO; Cat. No. ZB-2305; 1:2000), IPKine mouse anti-rabbit IgG light

chain secondary antibody, HRP-conjugated (Abbkine, Wuhan, China; Cat. No. A25022; 1:2000), or anti-rabbit IgG for IP, HRP-conjugated (Vazyme, Nanjing, China; Cat. No. RA1008-01; 1:3000) was used as appropriate. Input lysates and IgG immunoprecipitation were used as controls.

Statistical analysis

Statistical analyses were performed with GraphPad Prism 10.0 and R 4.2.0. Quantitative data are presented as mean ± SD. Unpaired t tests were used for comparisons between two independent groups, whereas paired t tests were applied to matched clinical tissues. For comparisons among three or more groups without a time variable, one-way ANOVA followed by Tukey's post hoc test was used. For comparisons among multiple groups with repeated measurements over time, such as CCK-8 time-course assays, two-way repeated-measures ANOVA followed by Tukey's multiple comparisons test was used. All in vitro assays were repeated at least three times independently. A two-sided $P < 0.05$ was considered statistically significant.

Results

Integrated single-cell and bulk RNA-seq analysis identifies lactate metabolism-related candidate genes in COAD

To screen lactate metabolism-related candidate genes relevant to colon adenocarcinoma, we first analyzed the colorectal cancer single-cell transcriptome dataset GSE231559 as a reference dataset. After dimensionality reduction and clustering, 17 cell clusters were identified in the UMAP plot. These clusters were annotated using known marker genes and assigned to major cell types, including T/NK cells, epithelial cells, monocytes/macrophages, B cells, fibroblasts, plasma cells, endothelial cells, and mast cells (**Figure 1A-C**). We then compared the Lac score among different cell types. Epithelial cells showed a higher Lac score than the other main cell populations ($P < 0.001$) (**Figure 1D**). This result suggested that epithelial cells in this single-cell reference dataset exhibited more active transcriptional features related to lactate metabolism. Differential expression analysis between these two groups identified 2,305 marker genes associated with lactate metabolism, which were subsequently used for further candidate gene selection. WGCNA identified 10 co-expression modules. Of these, the pink module, containing 64 genes and showed the strongest positive correlation with the Lac score ($r = 0.65$, $P = 2 \times 10\text{-}17$) (**Figure 1E**).

To identify candidate genes with high relevance to COAD, we performed an integrative screening by intersecting three gene sets: lactate metabolism marker genes from epithelial cells in the CRC single-cell reference dataset, differentially expressed genes from the TCGA-COAD cohort, and genes from the Lac score-related WGCNA module in TCGA-COAD. This integrative screening identified 14 lactate metabolism-related candidate genes, as shown in the Venn diagram (**Figure 1F**). Further expression analysis showed that these 14 genes had distinct expression patterns in COAD (**Figure 1G**). However, the heatmap mainly visualizes expression patterns and was not the sole basis for candidate selection. To improve the transparency of the prioritization process, the 14 genes were further evaluated according to tumor-upregulated expression, retention in the integrated screening strategy, biological relevance, STRING-predicted protein association, and feasibility for downstream experimental validation (Table S1). Among these candidates, RPS2 and EEF1B2 showed relatively consistent tumor-upregulated patterns and were both functionally related to the protein translation machinery. In addition, STRING prediction suggested a potential protein-level association between RPS2 and EEF1B2 (**Figure 1H**). Based on this convergent evidence, RPS2 and EEF1B2 were selected for subsequent clinical validation and functional assays. The remaining 12 genes are not biologically irrelevant, but they were not prioritized because their supporting evidence was less consistent with our Co-IP/rescue-based validation framework.

RPS2 and EEF1B2 are upregulated in public datasets and colon adenocarcinoma tissues

To further examine the expression profiles of RPS2 and EEF1B2 in colon adenocarcinoma, we compared their expression levels using a TCGA- and GTEx-based public platform that included 275 COAD tumor samples and 349

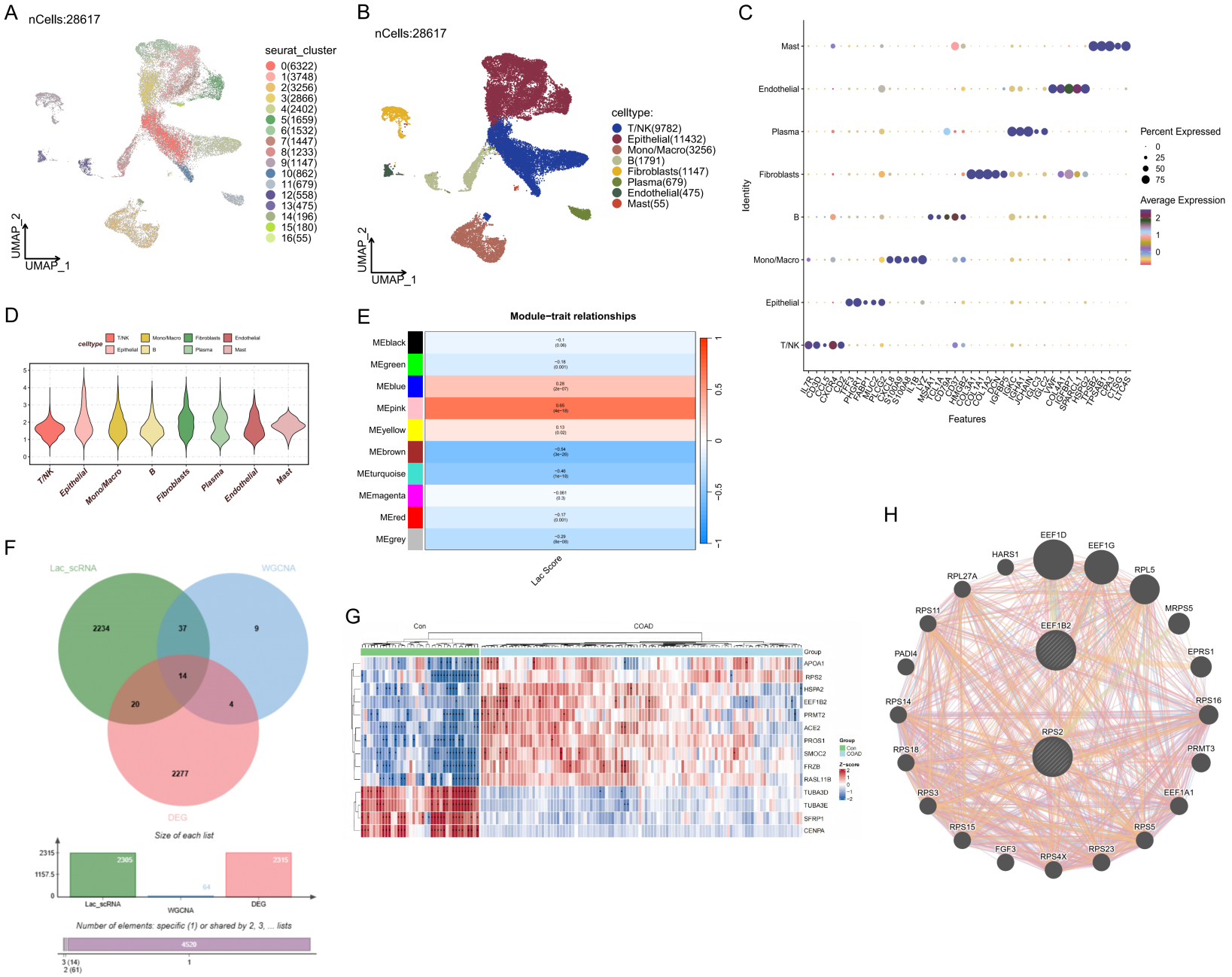
A
nCells:28617
seurat_cluster
0(6322)
1(3748)
2(3256)
3(2866)
4(2402)
5(1659)
6(1532)
7(1447)
8(1233)
9(1147)
10(862)
11(679)
12(558)
13(475)
14(196)
15(180)
16(55)
UMAP_2
UMAP_1
B
nCells:28617
celltype:
T/NK(9782)
Epithelial(11432)
Mono/Macro(3256)
B(1791)
Fibroblasts(1147)
Plasma(679)
Endothelial(475)
Mast(55)
UMAP_2
UMAP_1
C
Mast
Endothelial
Plasma
Fibroblasts
B
Mono/Macro
Epithelial
T/NK
Identity
Features
Percent Expressed
0
25
50
75
Average Expression
2
1
0
D
celltype
T/NK
Epithelial
Mono/Macro
B
Fibroblasts
Plasma
Endothelial
Mast
E
Module−trait relationships
MEblack
MEgreen
MEblue
MEpink
MEyellow
MEbrown
MEturquoise
MEmagenta
MEred
MEgrey
Lac Score
F
Lac_scRNA
WGCNA
DEG
2234
37
9
14
20
4
2277
Size of each list
2315
1157.5
0
2305
64
2315
Lac_scRNA
WGCNA
DEG
Number of elements: specific (1) or shared by 2, 3, ... lists
4520
3 (14)
2 (61)
1
G
Con
COAD
Group
APOA1
RPS2
HSPA2
EEF1B2
PRMT2
ACE2
PROS1
SMOC2
FRZB
RASL11B
TUBA3D
TUBA3E
SFRP1
CENPA
Z−score
H
EEF1D
EEF1G
HARS1
RPL27A
RPL5
RPS11
MRPS5
EEF1B2
PADI4
EPRS1
RPS14
RPS16
RPS2
RPS18
PRMT3
RPS3
EEF1A1
RPS15
RPS5
FGF3
RPS23
RPS4X

Figure 1. Integrated analysis of a colorectal cancer single-cell reference dataset and TCGA-COAD bulk RNA-seq data identified lactate metabolism-related candidate genes in COAD. A. UMAP plot showing the clustering distribution of cells in the GSE231559 colorectal cancer single-cell RNA-seq dataset after quality control, normalization, dimensionality reduction, and clustering. B. UMAP plot showing the annotated major cell populations, including T/NK cells, epithelial cells, monocytes/macrophages, B cells, fibroblasts, plasma cells, endothelial cells, and mast cells. C. Dot plot showing representative marker genes used for cell type annotation. D. Comparison of lactate metabolism scores among different cell types, showing relatively higher lactate metabolism-related transcriptional activity in epithelial cells. E. Module-trait relationship analysis from WGCNA in the TCGA-COAD cohort, showing the key module most strongly associated with the lactate metabolism score. F. Venn diagram showing the intersection of lactate metabolism-related marker genes from epithelial cells in the CRC single-cell reference dataset, differentially expressed genes from the TCGA-COAD cohort, and genes from the lactate score-related WGCNA module. G. Heatmap showing the expression patterns of the 14 lactate metabolism-related candidate genes in normal and COAD tissues from the TCGA-COAD cohort. H. STRING-based protein interaction network showing a potential association between RPS2 and EEF1B2 and their related interacting proteins.

normal samples. RPS2 expression was higher in tumor tissues than in normal tissues (**Figure 2A**). Similarly, EEF1B2 was also upregulated in tumor samples (**Figure 2B**).

To validate the protein expression patterns of RPS2 and EEF1B2, IHC was conducted using paired COAD and adjacent non-tumor tissues from 50 patients. Tumor sections exhibited more intense RPS2 immunostaining (**Figure 2C**). Consistently, semi-quantitative analysis of the stained area showed a higher RPS2-positive area ratio in tumor tissues (**Figure 2E**). A similar expression pattern was observed for EEF1B2. Its staining intensity was visibly increased in COAD tissues compared with adjacent tissues (**Figure 2D**), and quantitative analysis further showed an elevated EEF1B2-positive area ratio in tumor samples (**Figure 2F**).

Collectively, public database analysis and immunohistochemical validation showed that RPS2 and EEF1B2 were highly expressed in COAD. These findings provide both expression-level and histological evidence to support further investigation into their associations with malignant phenotypes and glycolysis-related changes in colon adenocarcinoma.

RPS2 and EEF1B2 downregulation suppresses proliferation and migration and promotes apoptosis in HT-29 cells

To investigate the functional relevance of RPS2 and EEF1B2 in COAD cells, HT-29 cells were individually silenced for RPS2 or EEF1B2, and a combined knockdown group was also generated. qPCR confirmed reduced RPS2 mRNA in the si-RPS2 group and decreased EEF1B2 mRNA in the si-EEF1B2 group; both transcripts were downregulated in the combined knockdown group (**Figure 3A**). Western blotting further verified the reduction of corresponding proteins in each silencing group (**Figure 3B**), confirming adequate transfection efficiency for subsequent experiments.

The CCK-8 assay indicated that suppression of either RPS2 or EEF1B2 reduced HT-29 cell viability relative to the si-NC group. This inhibitory effect was more pronounced when both genes were knocked down simultaneously (**Figure 3C**). Annexin V/PI flow cytometry further showed that single knockdown of RPS2 or EEF1B2 increased the apoptotic fraction of HT-29 cells, whereas combined knockdown produced a stronger pro-apoptotic effect (**Figure 3D**, **3E**). In the Transwell assay, fewer cells migrated through the membrane after RPS2 or EEF1B2 silencing, and the double-knockdown group showed the most marked reduction in migrated cell number (**Figure 3F**).

These findings indicate that RPS2 and EEF1B2 knockdown is associated with reduced proliferative and migratory capacities and enhanced apoptosis in HT-29 cells. The more pronounced changes observed after double knockdown suggest that both genes may contribute to HT-29 cell growth and migratory phenotypes.

RPS2 and EEF1B2 downregulation is accompanied by changes in apoptosis-related proteins and reduced glycolysis-related molecules

To further characterize the molecular changes after RPS2 and EEF1B2 knockdown, we assessed apoptosis- and glycolysis-related proteins. Compared with the si-NC group, Western blotting showed higher Bax and cleaved caspase-3 levels and lower Bcl-2 expression following RPS2 or EEF1B2 knockdown. These alterations were more pronounced when both genes were silenced (**Figure 4A**, **4B**). These observed protein changes were consistent with

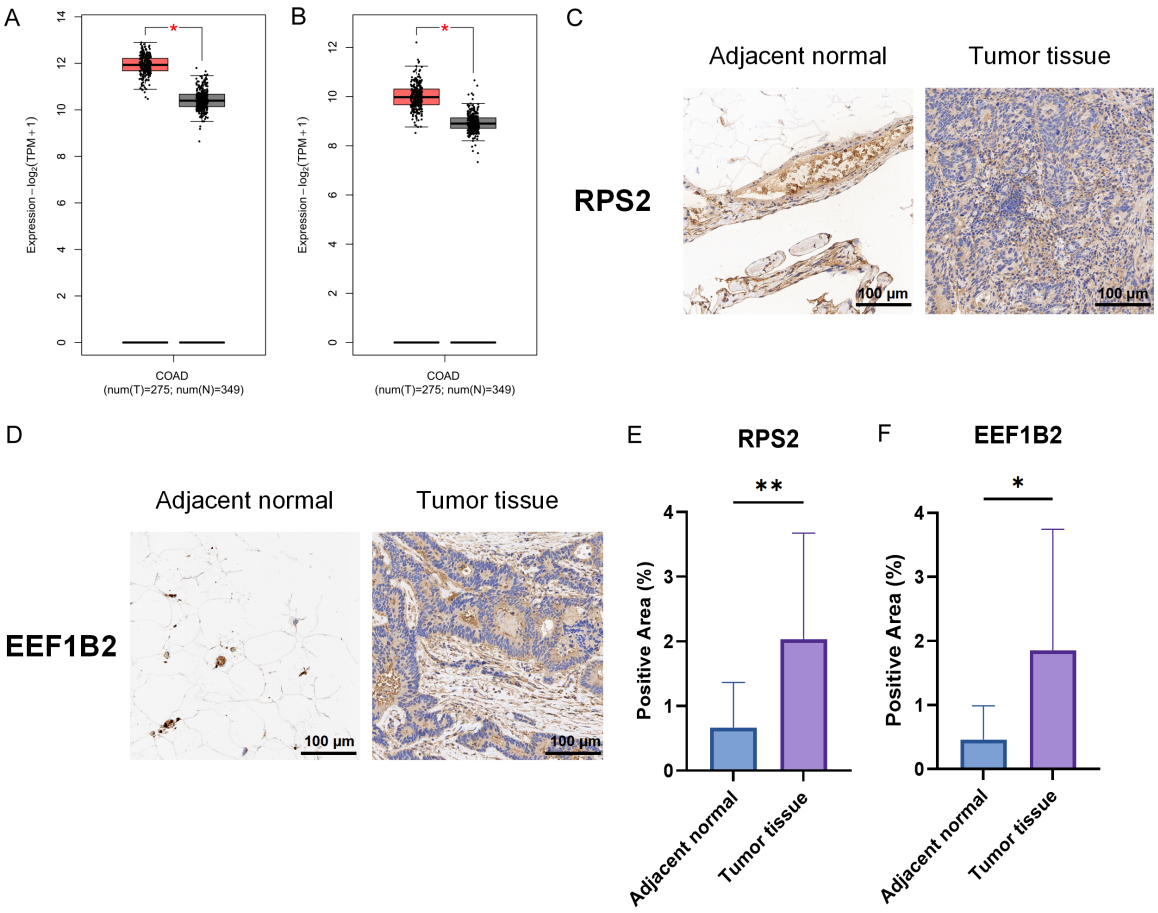

Figure 2. RPS2 and EEF1B2 were upregulated in public datasets and clinical colon adenocarcinoma tissues. A. Public database analysis showing higher RPS2 expression in COAD tumor tissues than in normal tissues. B. Public database analysis showing higher EEF1B2 expression in COAD tumor tissues than in normal tissues. C. Representative immunohistochemical staining images of RPS2 in colon adenocarcinoma tissues and matched adjacent normal tissues. Original magnification, ×200; scale bar, 100 μm. D. Representative immunohistochemical staining images of EEF1B2 in colon adenocarcinoma tissues and matched adjacent normal tissues. Original magnification, ×200; scale bar, 100 μm. E. Quantitative analysis of the RPS2-positive staining area ratio in tumor tissues and adjacent normal tissues. F. Quantitative analysis of the EEF1B2-positive staining area ratio in tumor tissues and adjacent normal tissues. Data are presented as mean ± SD. Statistical significance was determined using a paired t test. *P < 0.05, **P < 0.01.

flow cytometry results, suggesting that RPS2 and EEF1B2 downregulation increased apoptosis in HT-29 cells. We then measured the expression of glycolysis-related molecules. Western blot results showed reduced protein levels of HK2, PFK1, PKM2, and LDHA after RPS2 or EEF1B2 knockdown, with a stronger decrease observed in the double-knockdown group (**Figure 4C**, **4D**). qPCR analysis also indicated an overall reduction in the mRNA levels of these glycolysis-related genes (**Figure 4E**). Collectively, these findings demonstrate that RPS2 and EEF1B2 downregulation is associated with altered apoptosis-related proteins and decreased expression of several glycolysis-related molecules.

RPS2 knockdown is accompanied by reduced EEF1B2 protein expression and glycolysis-related metabolic changes

Based on the functional changes observed after combined knockdown, we further explored the relationship between RPS2 and EEF1B2 in HT-29 cells. Co-IP assays were initially performed to determine if these two proteins were associated at the protein level. EEF1B2 was detected in immunoprecipitates obtained with the RPS2 antibody, and reciprocally, RPS2 was detected in immunoprecipitates pulled down with the EEF1B2 antibody (**Figure 5A**, **5B**). These reciprocal co-IP results indicate that RPS2 and EEF1B2 may be present in the same

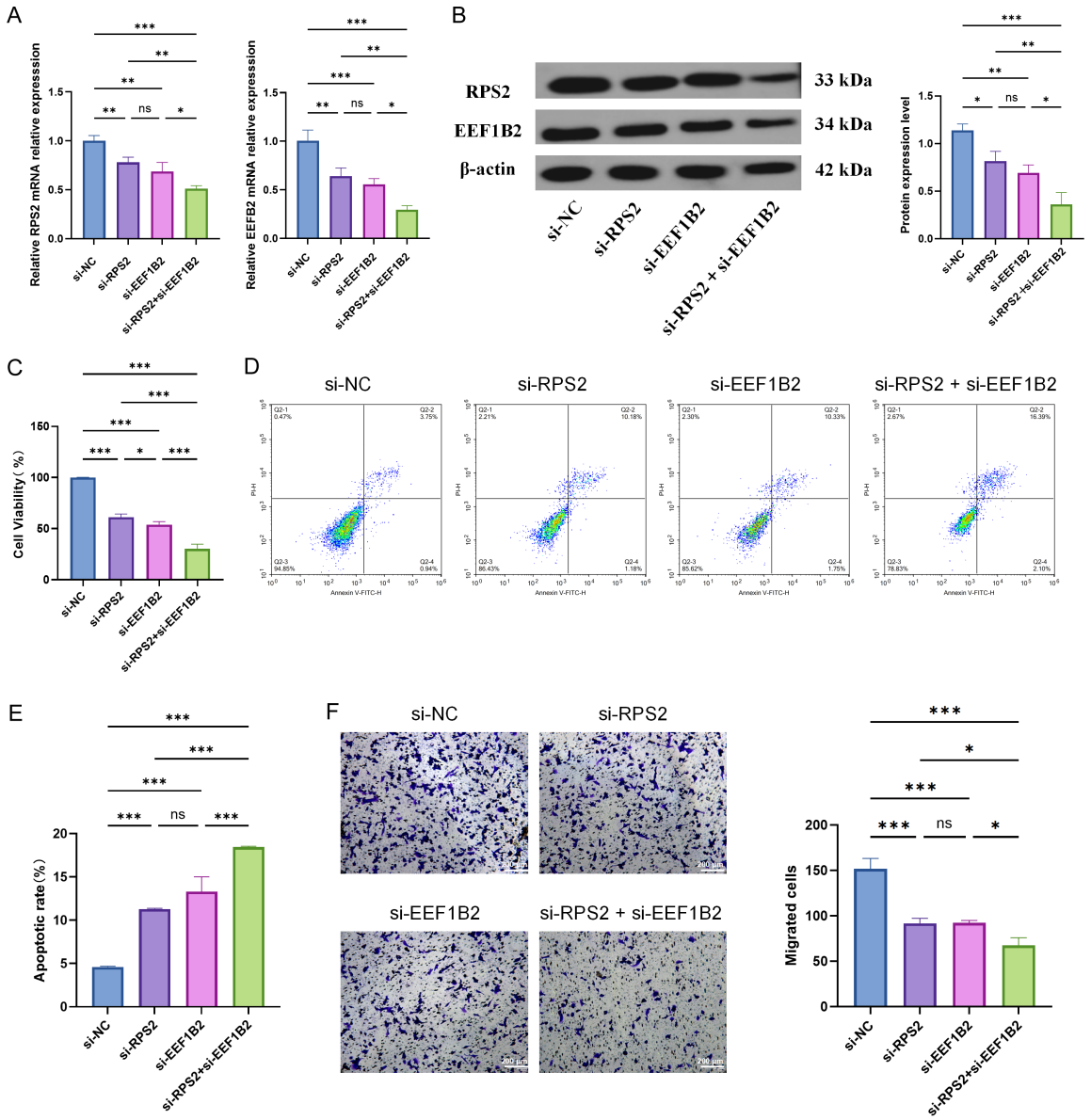

Figure 3. Knockdown of RPS2 and EEF1B2 suppressed proliferation and migration and promoted apoptosis in HT-29 cells. A. qPCR analysis confirming the knockdown efficiency of RPS2 and EEF1B2 in HT-29 cells transfected with si-NC, si-RPS2, si-EEF1B2, or si-RPS2 + si-EEF1B2. B. Representative Western blot bands and densitometric quantification of RPS2 and EEF1B2 protein expression after single or double knockdown. β-actin was used as the loading control. Quantification was performed from three independent experiments and normalized to β-actin. C. CCK-8 assay showing time-dependent changes in cell viability after RPS2 knockdown, EEF1B2 knockdown, or double knockdown. D. Representative flow cytometry plots of Annexin V-FITC/PI staining in the indicated groups. E. Quantitative analysis of the apoptosis rate based on flow cytometry. F. Representative images and quantitative analysis of Transwell migration assays in the indicated groups. Original magnification, ×100; scale bar, 200 μm. Data are presented as mean ± SD from at least three independent experiments. For the CCK-8 time-course assay, statistical analysis was performed using two-way repeated-measures ANOVA followed by Tukey's multiple comparisons test. For qPCR, Western blot quantification, apoptosis, and migration assays, statistical analysis was performed using one-way ANOVA followed by Tukey's post hoc test. Statistical comparisons are indicated by horizontal lines. *P < 0.05, **P < 0.01, and ***P < 0.001; ns, not significant.

protein-containing complex in HT-29 cells. Next, we investigated whether RPS2 knockdown was accompanied by changes in EEF1B2 protein expression. WB analysis showed that EEF1B2 protein expression decreased after RPS2 knockdown compared with the si-NC group (**Figure**

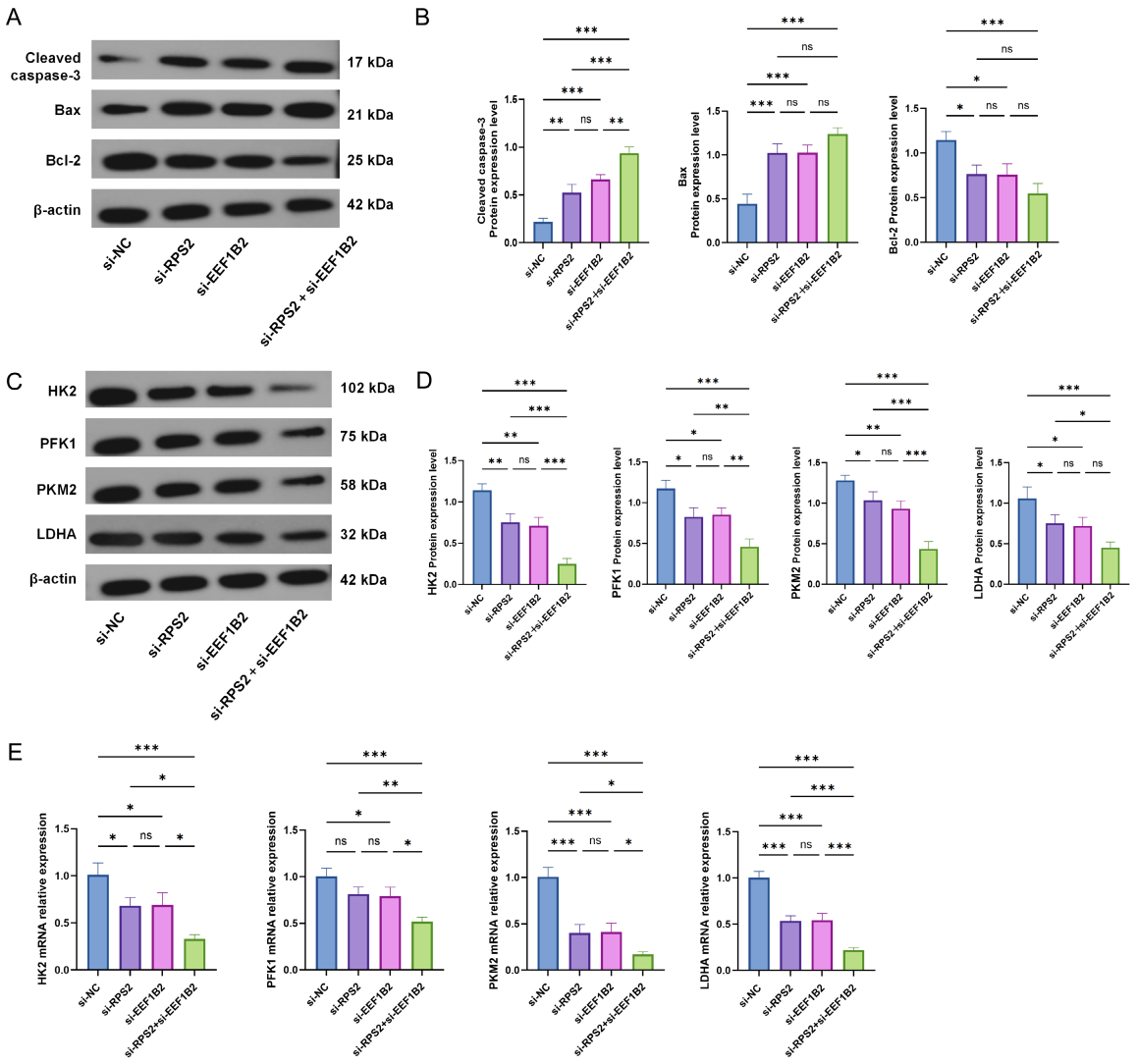

Figure 4. Downregulation of RPS2 and EEF1B2 was accompanied by changes in apoptosis-related proteins and glycolysis-related molecules in HT-29 cells. A. Representative Western blot bands showing the expression of apoptosis-related proteins, including Bax, Bcl-2, and cleaved caspase-3, in HT-29 cells transfected with si-NC, si-RPS2, si-EEF1B2, or si-RPS2 + si-EEF1B2. β-actin was used as the loading control. B. Semi-quantitative analysis of Bax, Bcl-2, and cleaved caspase-3 protein expression in the indicated groups. C. Representative Western blot bands showing the expression of glycolysis-related proteins, including HK2, PFK1, PKM2, and LDHA, in the indicated groups. β-actin was used as the loading control. D. Semi-quantitative analysis of HK2, PFK1, PKM2, and LDHA protein expression in the indicated groups. E. qPCR analysis of the relative mRNA expression levels of HK2, PFK1, PKM2, and LDHA in the indicated groups. Data are presented as mean ± SD from at least three independent experiments. Statistical analysis was performed using one-way ANOVA followed by Tukey's post hoc test. Statistical comparisons are indicated by horizontal lines. *P < 0.05, **P < 0.01, and ***P < 0.001; ns, not significant.

5C). This result indicates that RPS2 knockdown was accompanied by reduced EEF1B2 protein expression. However, this observation does not determine whether RPS2 directly regulates EEF1B2 protein abundance or whether the decrease in EEF1B2 reflects an indirect cellular response. We further assessed glucose- and lactate-related metabolic changes in the culture medium. Compared with the si-NC group, RPS2 knockdown led to higher residual glucose levels in the culture medium and lower lactate release, suggesting changes in glucose and lactate readouts consistent with reduced glycolysis-related activity (**Figure 5D**). These results indicate that RPS2 downregulation was accompanied by changes in glucose and lactate readouts, consistent with reduced glycolysis-related activity. Taken together, RPS2 and EEF1B2 were detected in the same protein complex in HT-29 cells, and RPS2 knockdown

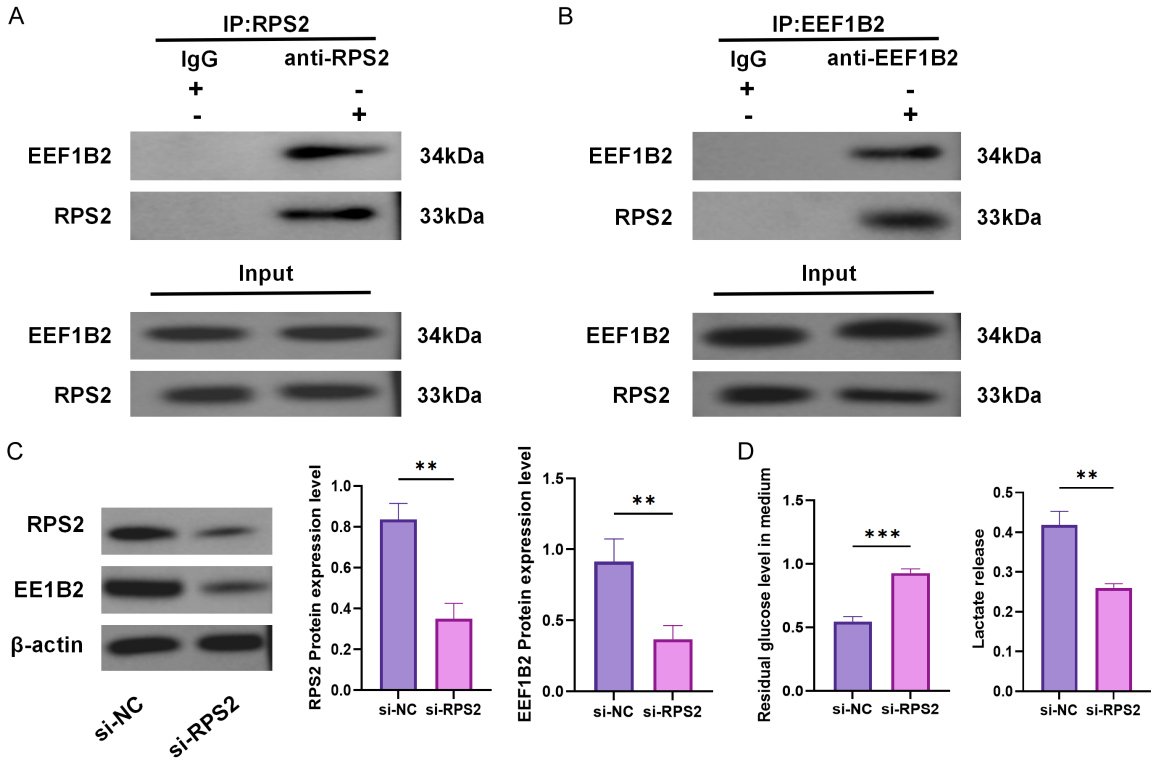

Figure 5. RPS2 and EEF1B2 were detected in the same protein complex, and RPS2 knockdown was accompanied by reduced EEF1B2 expression and changes in glucose and lactate readouts. A. Co-immunoprecipitation assay showing that EEF1B2 was detected in immunoprecipitates obtained with the anti-RPS2 antibody in HT-29 cells. IgG was used as the negative control, and input lysates were used as controls. B. Reciprocal co-immunoprecipitation assay showing that RPS2 was detected in immunoprecipitates obtained with the anti-EEF1B2 antibody in HT-29 cells. IgG was used as the negative control, and input lysates were used as controls. C. Western blot analysis showing that RPS2 knockdown was accompanied by decreased EEF1B2 protein expression in HT-29 cells. β-actin was used as the loading control. D. Measurement of glucose- and lactate-related metabolic changes in the culture medium after RPS2 knockdown. RPS2 knockdown increased the residual glucose level in the culture medium and reduced lactate release, suggesting glycolysis-related metabolic changes. Data are presented as mean ± SD from at least three independent experiments. Statistical significance was determined using an unpaired t test. **P < 0.01 and ***P < 0.001 versus si-NC.

was accompanied by reduced EEF1B2 protein expression.

EEF1B2 partially rescues the effects of RPS2 knockdown

To further investigate whether EEF1B2 was involved in the functional changes after RPS2 downregulation, four groups were established: si-NC + Vector, si-RPS2 + Vector, si-RPS2 + oe-EEF1B2, and oe-EEF1B2 alone. qPCR and Western blot analyses showed that RPS2 expression was reduced in the si-RPS2 + Vector group compared with the si-NC + Vector group, and EEF1B2 expression also decreased. In the si-RPS2 + oe-EEF1B2 group, RPS2 remained at a low level, whereas EEF1B2 expression was restored. When EEF1B2 was overexpressed alone, EEF1B2 expression increased, while RPS2 expression showed no obvious change (**Figure 6A**). The transfection results indicated that EEF1B2 was effectively overexpressed in HT-29 cells. Functional rescue assays were then performed to determine whether EEF1B2 could attenuate the effects caused by RPS2 silencing. In the CCK-8 assay, cells in the si-RPS2 + Vector group showed reduced viability compared with the control group. However, introducing EEF1B2 overexpression partly reversed this reduction in the si-RPS2 + oe-EEF1B2 group, although cell viability was still lower than that in the si-NC + Vector group (**Figure 6B**).

Flow cytometry analysis revealed a similar rescue trend. RPS2 knockdown increased the apoptotic rate in the si-RPS2 + Vector group,

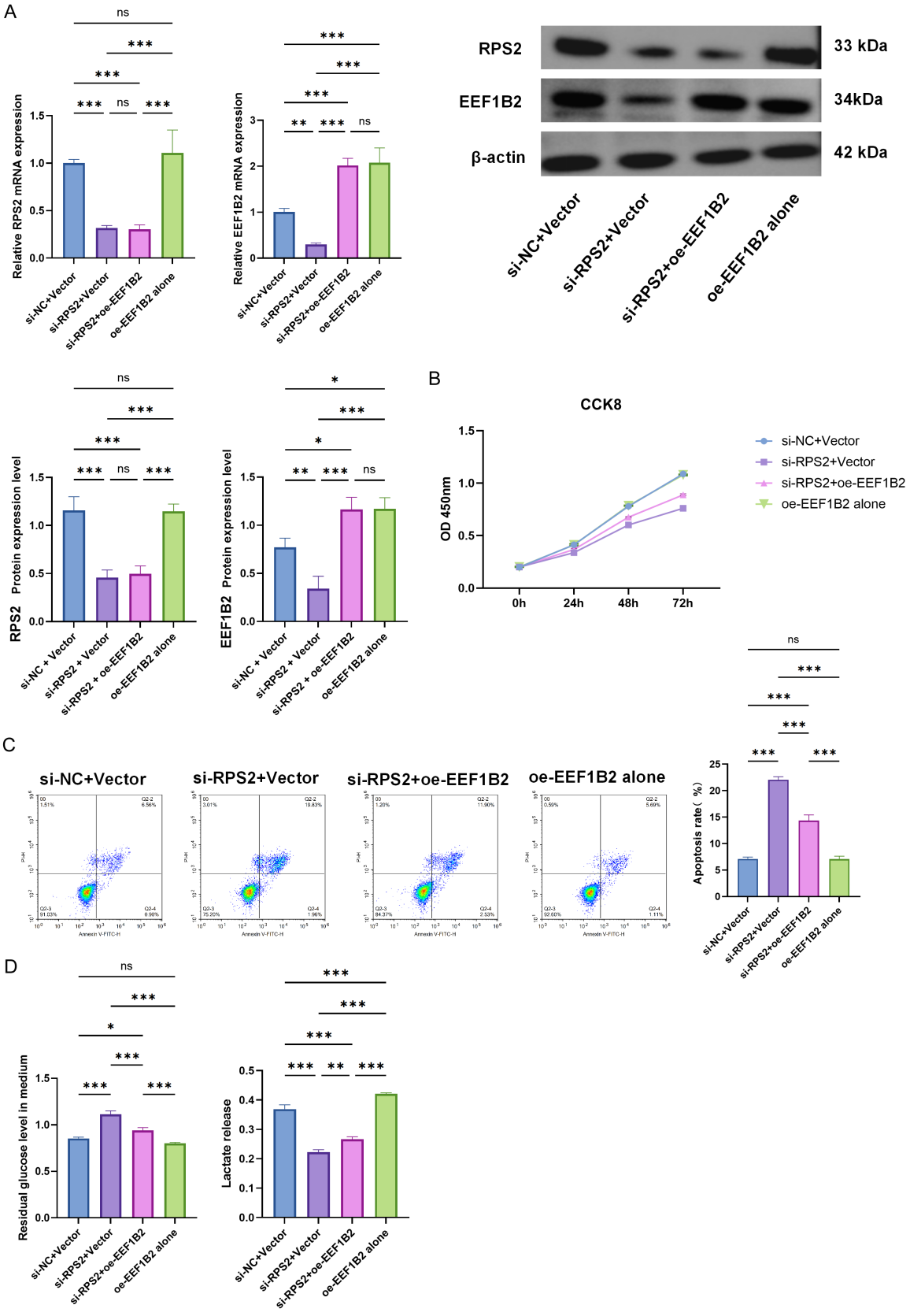

Figure 6. EEF1B2 overexpression partially rescued the effects of RPS2 knockdown in HT-29 cells. A. qPCR and Western blot validation of RPS2 knockdown and EEF1B2 overexpression. B. CCK-8 assay showing time-dependent partial

recovery of cell viability after EEF1B2 overexpression. C. Flow cytometric analysis of apoptosis in the indicated groups. D. Measurement of residual glucose levels and lactate release showing partial restoration of glycolysis-related metabolic changes. Data are presented as mean ± SD from at least three independent experiments. For the CCK-8 time-course assay, statistical analysis was performed using two-way repeated-measures ANOVA followed by Tukey's multiple comparisons test. For apoptosis and metabolic assays, statistical analysis was performed using one-way ANOVA followed by Tukey's post hoc test. Statistical comparisons are indicated by horizontal lines. *P < 0.05, **P < 0.01, and ***P < 0.001; ns, not significant.

whereas EEF1B2 overexpression partially decreased apoptosis. Nevertheless, the apoptosis level remained higher than that observed in the si-NC + Vector group (**Figure 6C**). We further evaluated glycolysis-related metabolic changes. Compared with control cells, the si-RPS2 + Vector group showed increased residual glucose in the culture medium and reduced lactate production. Upon EEF1B2 overexpression, glucose levels in the medium declined, while lactate release showed a partial recovery (**Figure 6D**). These findings suggest that EEF1B2 re-expression partly alleviated the decrease in cell viability, the increase in apoptosis, and the glycolysis-related metabolic changes observed after RPS2 knockdown. This partial rescue indicates that EEF1B2 may contribute to part of the RPS2 knockdown-related phenotype, but it does not prove direct regulation of EEF1B2 by RPS2 or a requirement for an intact RPS2/EEF1B2-containing complex.

Discussion

Tumor metabolic reprogramming, characterized by abnormal activation of aerobic glycolysis and excessive lactate accumulation, has been closely associated with malignant biological behaviors of colon adenocarcinoma (COAD), including invasion, metastasis, and immune escape. In this study, we focused on lactate metabolism-related transcriptional features and integrated single-cell transcriptome data with bulk RNA-seq data. Through this analysis, 14 lactate metabolism-related candidate genes were identified, and RPS2 and EEF1B2 were finally selected for systematic validation and functional investigation. Public database analysis and immunohistochemical validation in clinical tissues showed that both RPS2 and EEF1B2 were highly expressed in COAD. Further cell-based assays showed that reducing RPS2 or EEF1B2 expression altered the malignant phenotype of HT-29 cells. After knockdown, HT-29 cells displayed weaker proliferative and migratory abilities, a higher apoptotic rate, and lower levels of multiple glycolysis-associated molecules. The more pronounced phenotypic changes observed after double knockdown, together with the detection of RPS2 and EEF1B2 in the same protein complex, suggest that these two molecules may be related to glycolysis-associated malignant phenotypes in HT-29 cells.

At the single-cell level, tumor epithelial cells showed higher lactate metabolism scores than other cell populations, suggesting that tumor epithelial cells may show relatively active lactate metabolism-related transcriptional programs in CRC tissues. This result aligns with the concept that tumor parenchymal cells may modify the surrounding metabolic milieu through increased glycolytic activity [9, 12]. On this basis, RPS2 and EEF1B2 were screened by overlap analysis. These two genes were shared by three datasets: marker genes distinguishing epithelial cells with high versus low lactate metabolism scores in the single-cell analysis, differentially expressed genes between COAD tumors and normal tissues in TCGA, and genes from the WGCNA module most strongly correlated with the Lac score. This bioinformatics evidence suggests that RPS2 and EEF1B2 are closely associated with lactate metabolism-related transcriptional features in COAD. Functionally, RPS2 is a ribosomal small subunit protein, while EEF1B2 is a component of the translation elongation complex. Previous studies have shown that these molecules may have non-canonical functions beyond classical protein translation regulation and may participate in cell cycle progression, apoptosis regulation, migration, invasion, and tumor development [13, 14]. RPS2 has been reported to be upregulated in liver tumors and during liver regeneration, and its expression is closely related to cell proliferation [15]. EEF1B2 has been reported to facilitate abnormal MDSC recruitment and expansion in colorectal adenoma by regulating C/EBPβ protein synthesis [16]. These findings suggest that, in addition to classical glycolytic

rate-limiting enzymes and lactate transporters, some key molecules related to protein translation may be linked to tumor metabolic reprogramming. These findings supported the rationale for selecting RPS2 and EEF1B2 for further validation in the present study. Based on the above bioinformatics screening results and previous research evidence, we further verified the upregulation of RPS2 and EEF1B2 in COAD tissues using TCGA/GTEx-based public expression data and clinical specimens.

In the in vitro experiments evaluating the functional roles of RPS2 and EEF1B2, knockdown of either RPS2 or EEF1B2 reduced HT-29 cell proliferation and migration and promoted apoptosis. The inhibitory effects were more evident after double knockdown. These findings indicate that RPS2 and EEF1B2 may participate in sustaining malignant phenotype-related behaviors in HT-29 cells. However, although double knockdown produced a stronger inhibitory effect than single knockdown, the present data are not sufficient to confirm a true synergistic interaction between the two molecules.

To explore the molecular changes underlying these cellular effects, we further assessed apoptosis- and glycolysis-associated markers. Silencing RPS2 or EEF1B2 shifted the apoptotic profile of HT-29 cells, as shown by increased Bax and cleaved caspase-3 levels together with reduced Bcl-2 expression. In parallel, several glycolytic enzymes, including HK2, PFK1, PKM2, and LDHA were downregulated. These changes were generally more pronounced when RPS2 and EEF1B2 were knocked down simultaneously. Recent evidence also supports that glucose metabolic reprogramming is closely related to colorectal cancer proliferation, invasion, metastasis, and therapy resistance [17]. These results suggest that RPS2 and EEF1B2 downregulation was not only associated with weakened malignant phenotypes, but also accompanied by reduced expression of glycolysis-related molecules. HK2 has previously been reported to be upregulated in CRC, where it is linked to increased glycolytic activity and more active proliferative and migratory phenotypes [18]. PFK1 inhibition has been reported to reduce CRC cell proliferation and migration and may increase radiosensitivity, at least partly by suppressing glycolytic activity [19]. PKM2 is often upregulated in CRC and may contribute to tumor cell proliferation, migration, and STAT3-related signaling regulation [20, 21]. LDHA is commonly upregulated in CRC tissues, and its knockdown may decrease lactate and ATP generation, thereby limiting tumor growth. High LDH5/LDHA levels are also associated with invasive phenotypes and metastasis [22]. Together with our findings, these studies suggest that RPS2 and EEF1B2 may be related to the maintenance of glycolysis-associated states in COAD cells. However, whether this relationship is mediated by direct translational regulation, altered protein stability, or other indirect mechanisms still needs further investigation.

We further examined the possible relationship between RPS2 and EEF1B2 using Co-IP and rescue experiments. Co-IP showed that RPS2 and EEF1B2 could be detected in the same protein complex in HT-29 cells. However, this result does not prove a direct binary interaction between the two proteins. Because RPS2 is a ribosomal small subunit protein and EEF1B2 is a translation elongation factor-related protein, the detected complex may reflect their coexistence within a larger ribosome-associated or translation-related complex. It may also represent an indirect association mediated by other proteins or RNA molecules. The present study did not perform ribosome fractionation, RNase treatment, size-exclusion chromatography, mass spectrometry, proximity ligation assays, or domain-mapping experiments. Therefore, the composition and structural nature of the RPS2/EEF1B2-containing complex remain unclear. In addition, although RPS2 knockdown was accompanied by reduced EEF1B2 protein expression, increased residual glucose levels, and decreased lactate release, and EEF1B2 overexpression partially attenuated the effects of RPS2 knockdown on cell viability, apoptosis, and metabolic readouts, these findings do not explain how the RPS2/EEF1B2-containing complex affects malignant phenotypes. The current data support a possible functional connection between RPS2 and EEF1B2, but they do not define whether this connection depends on ribosomal translation, selective translation of glycolysis-related proteins, protein stability, RNA-mediated scaffolding, or other indirect mechanisms. Future studies should characterize the complex using ribosome profiling or polysome fractionation, RNase-sensitive co-IP,

mass spectrometry-based interactome analysis, and proximity-based validation methods. One apparent concern is that EEF1B2 overexpression partially rescued the effects of RPS2 knockdown, although RPS2 remained suppressed in this rescue setting. This finding should not be interpreted as restoration of a complete RPS2/EEF1B2-containing protein complex. Instead, it suggests that the reduction of EEF1B2 after RPS2 knockdown may contribute to part of the observed cellular effects. Because the rescue was partial rather than complete, RPS2 loss likely affects HT-29 cells through both EEF1B2-related and EEF1B2-independent mechanisms. In addition, EEF1B2 may exert some functions that do not require full restoration of RPS2 expression, possibly through its role in translation-associated processes or through indirect effects on proteins involved in cell survival and metabolic regulation. Therefore, the rescue experiment supports a functional contribution of EEF1B2 to the RPS2 knockdown phenotype, but it does not prove that an intact RPS2/EEF1B2 complex is required for these malignant phenotypes.

This study has several limitations. First, all in vitro functional experiments were performed in HT-29 cells. Although HT-29 is a commonly used colon cancer cell line, it has a specific molecular background and cannot represent the molecular diversity of COAD. Therefore, the current functional findings should be interpreted as HT-29 cell-based evidence rather than as general conclusions applicable to all COAD models. Validation in additional colon cancer cell lines with different genetic backgrounds is still required. Future studies should repeat key experiments, including RPS2/EEF1B2 knockdown, apoptosis analysis, migration assays, glycolysis-related marker detection, and rescue experiments, in other COAD cell lines, such as HCT116 cells with KRAS mutation or SW480 cells with APC mutation. Such validation would help determine whether the observed RPS2/EEF1B2-related phenotypes are conserved across different molecular subtypes of colon cancer. Second, although Co-IP and rescue assays suggested a possible functional relationship between RPS2 and EEF1B2, the specific mechanism by which RPS2 knockdown reduced EEF1B2 protein expression was not defined. This study did not examine EEF1B2 mRNA stability, protein half-life, ubiquitination status, or translation efficiency. Therefore, it remains unclear whether the decrease in EEF1B2 protein after RPS2 knockdown was caused by reduced mRNA stability, impaired translation, enhanced protein degradation, or an indirect cellular response. Future studies may use actinomycin D chase assays, cycloheximide chase assays, MG132 treatment, ubiquitination assays, polysome profiling, or reporter-based translation assays to clarify this regulatory mechanism. Furthermore, because EEF1B2 overexpression only partially rescued the RPS2 knockdown phenotype while RPS2 remained suppressed, the rescue results should not be interpreted as evidence that a complete RPS2/EEF1B2-containing complex was restored. These findings instead suggest that EEF1B2 may mediate only part of the downstream effects associated with RPS2 knockdown. Third, the assessment of glycolysis-related activity in this study was mainly based on indirect indicators, including glycolysis-related enzyme expression, residual glucose levels in the culture medium, and lactate release. Although these readouts are consistent with altered glucose metabolism, they cannot replace direct functional metabolic assays and cannot fully define changes in glycolytic flux. Residual glucose and lactate levels may also be influenced by differences in cell number, cell viability, medium consumption, or broader metabolic stress, even though normalization to total cellular protein was performed. Therefore, the current data should be interpreted as evidence of glycolysis-related changes rather than direct proof of altered glycolytic activity. Future studies should include more direct metabolic assays, such as Seahorse ECAR/OCR analysis, 2-NBDG glucose uptake assays, ATP production assays, or U-^{13}C-glucose isotope tracer analysis, to determine whether RPS2 and EEF1B2 directly affect glucose uptake, glycolytic flux, mitochondrial respiration, and carbon flow through glycolytic pathways. Fourth, this study did not perform glycolysis pathway-specific rescue experiments, such as HK2, PKM2, or LDHA overexpression after RPS2 or EEF1B2 knockdown. Therefore, the current data cannot determine whether reduced glycolysis is functionally responsible for the weakened malignant phenotypes observed after RPS2 or EEF1B2 knockdown. The decreases in cell proliferation and migration and the increase in apoptosis occ-

urred together with reduced glycolysis-related enzyme expression, increased residual glucose levels, and decreased lactate release. However, these parallel changes do not establish a causal relationship. Reduced glycolysis may contribute to the phenotypic effects, but it may also be a concomitant consequence of impaired cellular growth or broader metabolic stress. Future studies should include rescue experiments, such as RPS2 knockdown combined with HK2 or PKM2 overexpression, to determine whether restoration of glycolytic activity can reverse the inhibition of proliferation and migration or the increase in apoptosis. Finally, this study did not include animal experiments or larger clinical validation. Therefore, the actual roles of RPS2 and EEF1B2 in COAD growth, metastasis, and patient outcomes in vivo remain to be further investigated.

In summary, by integrating transcriptional features related to lactate metabolism, this study identified RPS2 and EEF1B2 as highly expressed genes in COAD and further supported their potential functional involvement. In HT-29 cells, silencing these genes was linked to reduced proliferative and migratory abilities, together with increased apoptosis, and reduced expression of several glycolysis-associated molecules. Co-IP results showed that RPS2 and EEF1B2 could be detected in the same protein complex, and rescue experiments further indicated that EEF1B2 may partly participate in the functional effects observed after RPS2 downregulation. Overall, this study provides preliminary evidence that RPS2 and EEF1B2 are associated with glycolysis/lactate metabolism-related malignant phenotypes in HT-29 cells. However, the specific molecular pathway by which RPS2 affects EEF1B2 protein expression and glycolysis-related changes remains to be determined. These findings provide a basis for future studies on the connection between translation-related molecules and metabolic reprogramming in colon adenocarcinoma.

Disclosure of conflict of interest

None.

Abbreviations

CRC, colorectal cancer; COAD, colon adenocarcinoma; IARC, International Agency for Research on Cancer; GEO, Gene Expression Omnibus; TCGA, The Cancer Genome Atlas; RNA-seq, RNA sequencing; scRNA-seq, single-cell RNA sequencing; ssGSEA, single-sample gene set enrichment analysis; WGCNA, weighted gene co-expression network analysis; UMAP, Uniform Manifold Approximation and Projection; PCA, principal component analysis; UMI, unique molecular identifier; FDR, false discovery rate; log2FC, log2 fold change; IHC, immunohistochemistry; qPCR, quantitative real-time polymerase chain reaction; Co-IP, co-immunoprecipitation; FBS, fetal bovine serum; BSA, bovine serum albumin; PBS, phosphate-buffered saline; RIPA, radioimmunoprecipitation assay; BCA, bicinchoninic acid; SDS-PAGE, sodium dodecyl sulfate-polyacrylamide gel electrophoresis; PVDF, polyvinylidene fluoride; ECL, enhanced chemiluminescence; CCK-8, Cell Counting Kit-8; HRP, horseradish peroxidase; FITC, fluorescein isothiocyanate; PI, propidium iodide; DAB, diaminobenzidine; Bax, Bcl-2-associated X protein; Bcl-2, B-cell lymphoma 2; HK2, hexokinase 2; PFK1, phosphofructokinase 1; PKM2, pyruvate kinase M2; LDHA, lactate dehydrogenase A; MCT, monocarboxylate transporter; SD, standard deviation.

Address correspondence to: Jianbin Hou, Quanzhou First Hospital Affiliated to Fujian Medical University, No. 248-252 Dong Street, Quanzhou 362000, Fujian, China. E-mail: hhjianbb@126.com

References

[1] Bray F, Laversanne M, Sung H, Ferlay J, Siegel RL, Soerjomataram I and Jemal A. Global cancer statistics 2022: GLOBOCAN estimates of incidence and mortality worldwide for 36 cancers in 185 countries. CA Cancer J Clin 2024; 74: 229-263.

[2] Wang W, Lin X, Yu R, Zhou S, Liu Y, Jia H, Han F, Bu Y and Pu J. Down-regulated C4orf19 confers poor prognosis in colon adenocarcinoma identified by gene co-expression network. J Cancer 2022; 13: 1145-1159.

[3] Sedlak JC, Yilmaz OH and Roper J. Metabolism and colorectal cancer. Annu Rev Pathol 2023; 18: 467-492.

[4] Pang B and Wu H. Metabolic reprogramming in colorectal cancer: a review of aerobic glycolysis and its therapeutic implications for targeted treatment strategies. Cell Death Discov 2025; 11: 321.

[5] Wang J, Wang H, Liu A, Fang C, Hao J and Wang Z. Lactate dehydrogenase A negatively regulated by miRNAs promotes aerobic glycolysis

and is increased in colorectal cancer. Oncotarget 2015; 6: 19456-19468.
[6] Kim HK, Lee I, Bang H, Kim HC, Lee WY, Yun SH, Lee J, Lee SJ, Park YS, Kim KM and Kang WK. MCT4 expression is a potential therapeutic target in colorectal cancer with peritoneal carcinomatosis. Mol Cancer Ther 2018; 17: 838-848.
[7] Kumar A, Kant S and Singh SM. Targeting monocarboxylate transporter by alpha-cyano-4-hydroxycinnamate modulates apoptosis and cisplatin resistance of Colo205 cells: implication of altered cell survival regulation. Apoptosis 2013; 18: 1574-1585.
[8] Kim J and DeBerardinis RJ. Mechanisms and implications of metabolic heterogeneity in cancer. Cell Metab 2019; 30: 434-446.
[9] Zhong X, He X, Wang Y, Hu Z, Huang H, Zhao S, Wei P and Li D. Warburg effect in colorectal cancer: the emerging roles in tumor microenvironment and therapeutic implications. J Hematol Oncol 2022; 15: 160.
[10] Deng F, Zhou R, Lin C, Yang S, Wang H, Li W, Zheng K, Lin W, Li X, Yao X, Pan M and Zhao L. Tumor-secreted dickkopf2 accelerates aerobic glycolysis and promotes angiogenesis in colorectal cancer. Theranostics 2019; 9: 1001-1014.
[11] Qin R, Fan X, Huang Y, Chen S, Ding R, Yao Y, Wu R, Duan Y, Li X, Khan HU, Hu J and Wang H. Role of glucose metabolic reprogramming in colorectal cancer progression and drug resistance. Transl Oncol 2024; 50: 102156.
[12] Steeghs JPJM, Offermans K, Jenniskens JCA, Samarska I, Fazzi GE, van den Brandt PA and Grabsch HI. Relationship between the Warburg effect in tumour cells and the tumour microenvironment in colorectal cancer patients: results from a large multicentre study. Pathol Res Pract 2023; 247: 154518.
[13] El Khoury W and Nasr Z. Deregulation of ribosomal proteins in human cancers. Biosci Rep 2021; 41: BSR20211577.
[14] Pk S, Freimanis J, Kovala T and Parissenti AM. Extra-ribosomal roles for ribosomal proteins and their relevance to tumour suppression, carcinogenesis and cancer progression. Cancers (Basel) 2025; 17: 2825.
[15] Kowalczyk P, Woszczynski M and Ostrowski J. Increased expression of ribosomal protein S2 in liver tumors, posthepactomized livers, and proliferating hepatocytes in vitro. Acta Biochim Pol 2002; 49: 615-624.
[16] Pan J, Zhao L, Du H, Zhu Y, Sun X, Xu Q, Cheng H, Chen H and Sun Y. Cannabidiol suppresses emergency MDSCs generation by disturbing EEF1B2-mediated C/EBPbeta protein synthesis in colorectal adenomas. J Immunother Cancer 2026; 14: e013081.
[17] Zhou R, Wang F, Wen J, Zhou X and Wen Y. Glucose metabolic reprogramming in colorectal cancer: from mechanisms to targeted therapy approaches. Cancer Med 2025; 14: e71185.
[18] Katagiri M, Karasawa H, Takagi K, Nakayama S, Yabuuchi S, Fujishima F, Naitoh T, Watanabe M, Suzuki T, Unno M and Sasano H. Hexokinase 2 in colorectal cancer: a potent prognostic factor associated with glycolysis, proliferation and migration. Histol Histopathol 2017; 32: 351-360.
[19] Tian RF, Li XF, Xu C, Wu H, Liu L, Wang LH, He D, Cao K, Cao PG, Ma JK and Huang CH. SiRNA targeting PFK1 inhibits proliferation and migration and enhances radiosensitivity by suppressing glycolysis in colorectal cancer. Am J Transl Res 2020; 12: 4923-4940.
[20] Yang P, Li Z, Fu R, Wu H and Li Z. Pyruvate kinase M2 facilitates colon cancer cell migration via the modulation of STAT3 signalling. Cell Signal 2014; 26: 1853-1862.
[21] Huang X, He J, Sun H, Wu Y, Gu R and Li Z. PKM2-driven metabolic reprogramming in digestive system tumors: mechanisms, therapeutic advances, and clinical challenges. Front Immunol 2025; 16: 1634786.
[22] Ngamkham J, Moungthard H, Thesawadwomg T, Mus UDM, Phansri T, Boonmark K and Phukhan T. Clinical significance of lactate dehydrogenase A expression in colorectal cancer. Cureus 2025; 17: e98628.

Table S1. Prioritization rationale for the 14 lactate metabolism-related candidate genes

Candidate gene	Main biological relevance	STRING/network or validation relevance	Prioritization decision
APOA1	Lipid transport and metabolic regulation; may be linked to tumor metabolism and systemic metabolic status	Not selected as a paired protein-interaction candidate for the current RPS2/EEF1B2-focused validation strategy	Not prioritized in this study
RPS2	Ribosomal small subunit protein; related to protein translation, cell proliferation, and tumor biology	Showed a predicted protein-level association with EEF1B2, providing a rationale for Co-IP and rescue experiments	Prioritized for validation
HSPA2	Heat shock protein family member; associated with protein folding, stress response, and tumor progression	Biologically relevant, but not selected because it did not provide the same paired translation-related validation framework as RPS2/EEF1B2	Not prioritized in this study
EEF1B2	Translation elongation-related protein; may be involved in tumor progression and protein synthesis regulation	Showed a predicted protein-level association with RPS2, supporting paired Co-IP and rescue validation	Prioritized for validation
PRMT2	Protein arginine methyltransferase; may regulate transcriptional and post-translational processes	Potentially relevant to tumor regulation, but outside the focused translation-related RPS2/EEF1B2 validation axis	Not prioritized in this study
ACE2	Peptidase and renin-angiotensin system-related molecule; may be linked to inflammation and epithelial biology	Did not fit the Co-IP/rescue-based paired validation framework used in this study	Not prioritized in this study
PROS1	Coagulation- and immune-related molecule; may participate in tumor microenvironment regulation	Biologically interesting, but less directly connected to the protein translation-related validation strategy	Not prioritized in this study
SMOC2	Extracellular matrix-associated protein; implicated in tumor invasion and stromal remodeling	Potentially relevant to tumor progression, but not selected for the current intracellular protein-complex validation design	Not prioritized in this study
FRZB	Secreted Wnt pathway modulator; may affect tumor signaling and epithelial behavior	Biologically relevant, but not prioritized because the current study focused on translation-related intracellular candidates	Not prioritized in this study
RASL11B	Small GTPase-like protein; may be involved in intracellular signaling	Functional relevance to glycolysis-associated phenotypes remains less established in the current screening context	Not prioritized in this study
TUBA3D	Tubulin family member; related to cytoskeletal organization and cell morphology	May be linked to cell behavior, but was not suitable for the specific RPS2/EEF1B2 Co-IP/rescue validation framework	Not prioritized in this study
TUBA3E	Tubulin family member; related to cytoskeletal organization and microtubule structure	Potentially associated with cell migration or structural regulation, but not selected for this translation-related validation axis	Not prioritized in this study
SFRP1	Secreted Wnt signaling antagonist; associated with epithelial signaling and tumor biology	Biologically relevant, but not selected because the current experimental framework focused on intracellular protein association and rescue	Not prioritized in this study
CENPA	Centromere protein; related to chromosome segregation, cell cycle, and tumor proliferation	Potentially relevant to proliferation, but not selected because it did not provide the same paired protein-complex rationale as RPS2/EEF1B2	Not prioritized in this study